Dynamic Modelling and Simulation of Planar Flexible-link Robots with Elastic Rotational Restraints at the Joint-Link Couplings

Francis Kunzi Tekweme

University of Johannesburg

ftekweme@uj.ac.za

Abstract

This paper presents the dynamic model of multilink flexible robot with elastic rotational restraints at the joint-link coupling. The proposed approach is flexible as it can mimic the classic clamped case model considering an infinite hinge rotational stiffness coefficient. The particular case of flapping motion is also a degenerate case of the proposed model where the stiffness coefficient is almost zero. Considering that most joint- link couplings are subject to some degree of elastic deformation, the proposed approach is flexible and suitable for modelling multilink flexible robots. Simulations were conducted to assess the effect of the elastic rotational constraints at the actuator gearhead shaft-link couplings. The simulation results demonstrated that the magnitudes of the relative motion at the actuator gearhead shaft- link couplings have a substantial influence on the vibration frequency of the planar flexible- link robot tip.

Keywords: Multilink; coupling; stiffness; hinge and rotational.

Nomenclature list

General Symbols

b_i	i^{th} link thickness
D	Damping matrix
d_i	Distance of center of mass of link i from joint i axis
E_i	Young modulus of link i
$(EI)_i$	Flexural rigidity of link i
f_i	Vector generalized forces
h_i	Coriolis and centrifugal forces vector elements
h_{ti}	Height of link i
I_i	second moment of area about the neutral axis of cross section of link i
J_{hi}	moment of inertia of hub i
J_{Li}	Actual moment of inertia at the distal end of link i
J_{oi}	Moment of inertia of link i about joint i axis
J_p	Payload inertia
J_{vi}	The 2 x 6 Jacobian matrix relating the linear velocity of a point located at x_i along link i to the general coordinates
$J_{\omega i}$	The 2 x 6 Jacobian matrix relating the angular velocity of a point located at x_i along link i to the general coordinates
K	Flexible- link system stiffness matrix
K_{ijk}	j^{th} row and k^{th} column element of the stiffness matrix diagonal block relative to link i
L	Lagrangian
l_i	Length of link i
$M(q)$	Inertia matrix
m_{hi}	Hub i mass
m_i	Link i mass
M_{ij}	i^{th} row and j^{th} column inertia matrix element
M_{Li}	Actual mass at the distal end of link i
m_p	Payload mass
$(MD)_i$	Contribution of masses non-collocated at the distal end of link i
n	Number of flexible links
N	Number of selected general coordinates
$P_i(t)$	Position vector of a point along the deflected link with respect to inertial frame
P_i	Scale factor (i.e., normalizing constant)
$\dot{P(t)}$	Absolute linear velocity
Q	Input weighting matrix
$\{q(t)\}$	Generalized coordinates vector
t	Time (continuous)
T	Total kinetic energy
u	n- vector of joint torques
V	Total potential energy
x_i	Distance from hub i along link i
$(X_i\ Y_i)$	Rigid body moving frame associated to link i
(X_0, Y_0)	Inertial frame
$y_i(x_i)$	Transversal deflection of link i at abscissa x_i

$Y_i(x_i,t)$	Transversal deflection of link i at abscissa x_i and time t
y_{ie}	Transversal deflection of link i at the distal end of link i
y'_{ie}	Slope of the deflection of neutral axis at the distal end of link i with respect to the abscissa axis of the rigid body moving frame associated to link i
y'_{io}	Slope of the deflection of neutral axis at the proximal end of link i with respect to the abscissa axis of the rigid body moving frame associated to link i.

Greek Symbols

β	Relative rotation angle between link 1 and link 2
$\delta_{ij}(t)$	Time varying variable associated with the assumed modes shape $\phi_{ij}(x_i)$ of link i
$\theta_i(t)$	Rigid motion (joint angle) of link i
$\dot{\theta}_i(t)$	Hub i angular velocity
ρ_i	Mass per unit length of link i
σ_{oti}	Torsional stiffness coefficient of joint- link is
ϖ_{ij}	Link i deformation moments of order 1 of mode j.
Z_{ijk}	Link i cross moments of modes j and k.

1. Introduction

Most dynamic models for multilink flexible robots derived from the assumed mode methods considered each of the connections between the link and the actuator gearhead shaft fully clamped. However, [1] stressed that in reality, connections behave neither as perfect clamped end nor as perfect-hinged end. He recommended the use of semi-rigid connections that capture the true behaviour of the joints. In attempting to derive a more accurate dynamic model, [2] used torsional spring to describe the joint flexibility. However, he considered the classical clamped end formulation at each of the actuator gearhead shaft-link connections and found that the natural frequencies were slightly overestimated. [3] studied the eigenfunctions for a flexible slewing link using two distinct formulations of the boundary conditions, namely, pseudo-clamped and pseudo-pinned. They showed that the two approaches were equivalent and lead to the same results. In this paper, each of the actuator gearhead shaft-link connections is modelled as torsional spring, which covers the full range of flexibility from frictionless hinged to clamped end. The simulation results are reported to show the influence of the spring stiffness coefficient on the vibrational behaviour of the planar two-link flexible robot tip.

2. Kinematic modelling

Prior to kinematic and dynamic analysis of the flexible link of uniform density, some useful constant and variable parameters that are extensively used need to be defined [4]:

$$m_i = \int_0^{l_i} \rho_i dx_i = \rho_i l_i \tag{1.a}$$

$$\varpi_{ij} = \int_0^{l_i} \rho_i \phi_{ij}(x_i) x_i dx_i \tag{1b}$$

$$d_i = \frac{1}{m_i}\int_0^{l_i} \rho_i x_i dx_i = \frac{1}{2} l_i \tag{1c}$$

$$z_{ijk} = \int_0^{l_i} \rho_i \phi_{ij}(x_i)\phi_{ik}(x_i) dx_i \tag{1d}$$

$$J_{0i} = \int_0^{l_i} \rho_i x_i^2 dx_i = \frac{1}{3} m_i l_i^2 \tag{1e}$$

Consider a two-link flexible robot with rotational elastic restraint at each actuator gearhead shaft-link coupling. The rotating frame (X_i, Y_i) is defined such that the abscissa axis (X_i) is tangent to the link at the base when the rotational stiffness tends to infinite (i.e. clamped mass case) as shown in Fig. 1 and 2. Both figures are adapted from [5].

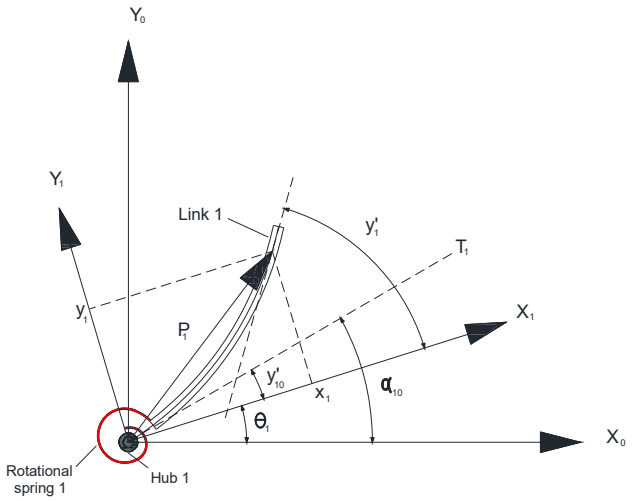

Fig. 1. Position vector P_1 of a point on link 1

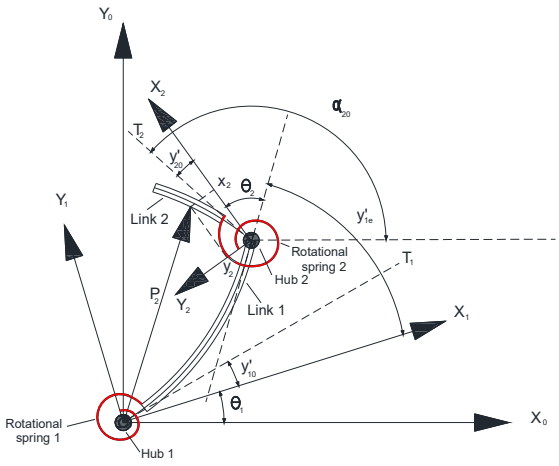

Fig. 2. Position vector P_2 of a point on link 2.The position vectors P_1 and P_2 with respect to the inertial frame (X_0 ,Y_0) are expressed as follows [5]

$$P_1 = \begin{bmatrix} P_{1x1} \\ P_{1y1} \end{bmatrix} \quad \text{and} \quad P_2 = \begin{bmatrix} P_{2x2} \\ P_{2y2} \end{bmatrix} \tag{2}$$

where $P_{1x1} = x_1 \cos\theta_1 - y_1 \sin\theta_1$ and $P_{1y1} = x_1 \sin\theta_1 + y_1 \cos\theta_1$

$$P_{2x2} = l_1 \cos\theta_1 - y_{ie} \sin\theta_1 + x_2 \cos(\theta_1 + \theta_2) - x_2 \sin(\theta_1 + \theta_2) y'_{1e} - y_2 \sin(\theta_1 + \theta_2) - y_2 \cos(\theta_1 + \theta_2) y'_{1e}$$

$$P_{2y2} = l_1 \sin\theta_1 + y_{ie} \cos\theta_1 + x_2 \sin(\theta_1 + \theta_2) + x_2 \cos(\theta_1 + \theta_2) y'_{1e} + y_2 \cos(\theta_1 + \theta_2) - y_2 \sin(\theta_1 + \theta_2) y'_{1e}$$

The absolute rotation angle of the bracket located at the base of link 1 is given by

$$\alpha_{10} = \theta_1(t) + y'_{10} \tag{3}$$

When $y'_{10} = 0$, equation (3) represents the absolute rotation angle of bracket of link 1 for the clamped case. The absolute rotation angle of the bracket located at the base of link 2 is expressed as

$$\alpha_{20} = \theta_1(t) + \theta_2(t) + y'_{1e} + y'_{20} \tag{4}$$

Equation (4) agrees with the one for a clamped case when $y'_{20} = 0$.

The relative rotation angle (β) between links 1 and 2, measured between the tangent to the neutral axis of link 1 distal end and the tangent to the neutral axis of link 2 basis is given by

$$\beta = y'_{20} + \theta_2 \tag{5}$$

The relative rotation angle between links 1 and 2 are obtained by setting $y'_{20} = 0$ in equation (5).

To obtain a finite dimensional model the assumed modes method can be used. Therefore the elastic transversal deflections y_1 and y_2 can be evaluated as functions of spatial mode shapes $\phi_{ij}(x_i)$ and time dependent general coordinates $\delta_{ij}(t)$. Considering two dominant modes per link yields

$$y_1(x_1,t) = \phi_{11}(x_1)\delta_{11}(t) + \phi_{12}(x_1)\delta_{12}(t) \quad \text{and} \quad y_2(x_2,t) = \phi_{21}(x_2)\delta_{21}(t) + \phi_{22}(x_2)\delta_{22}(t) \tag{6}$$

Six generalized coordinates can be used to completely describe the motion of a two-link flexible robot arm. The

vector of generalized coordinates can be expressed as

$$q(t)=[\theta_1(t),\theta_2(t),\delta_{11}(t),\delta_{12}(t),\delta_{21}(t),\delta_{22}(t)]^T \tag{7}$$

3. Dynamic modelling

The mode shapes can be derived from the solution to the partial differential equation

$$(EI)_i\frac{\partial^4 y_i(x_i,t)}{\partial x_i^4}+\rho_i\frac{\partial^2 y_i(x_i,t)}{\partial t^2}=0,\quad i=1,2. \tag{8}$$

and the boundary conditions are [5]

$$y_i(0,t)=0\ .\ i=1,2 \tag{9}$$

$$(EI)_i\frac{\partial^2 y_i(x_i,t)}{\partial x_i^2}\bigg|_{x_i=0}=\sigma_{oti}\left(\frac{\partial y_i(x_i,t)}{\partial x_i}\bigg|_{x_i=0}\right) \tag{10}$$

$$(EI)_i\frac{\partial^2 y_i(x_i,t)}{\partial x_i^2}\bigg|_{x_i=l_i}=-J_{Li}\frac{d^2}{dt^2}\left(\frac{\partial y_i(x_i,t)}{\partial x_i}\bigg|_{x_i=l_i}\right)-(MD)_i\frac{d^2}{dt^2}\left(y_i(x_i,t)\big|_{x_i=l_i}\right)\quad i=1,2 \tag{11}$$

$$(EI)_i\frac{\partial^3 y_i(x_i,t)}{\partial x_i^3}\bigg|_{x_i=l_i}=M_{Li}\frac{d^2}{dt^2}\left(y_i(x_i,t)\big|_{x_i=l_i}\right)+(MD)_i\frac{d^2}{dt^2}\left(\frac{\partial y_i(x_i,t)}{\partial x_i}\bigg|_{x_i=l_i}\right)\ldots..\ i=1,2 \tag{12}$$

where $M_{L1}=m_2+m_{h2}+m_p$, $M_{L2}=m_p$, $J_{L1}=J_{02}+J_{h2}+J_p+m_pl_2^2$, $J_{L2}=J_p$,

$(MD)_1=(m_2d_2+m_pl_2)\cos\theta_2-[(\nu_{21}+m_p\phi_{21e})\delta_{21}+(\nu_{22}+m_p\phi_{22e})\delta_{22}]\sin\theta_2$, $(MD)_2=0$

The frequency equation is given by [5]

$$\Delta_1+\frac{1}{\sigma_{oti}}\Delta_2=0 \tag{13}$$

where

$$\begin{aligned}\Delta_1=\{&1+\cos(\beta_il_i)\cosh(\beta_il_i)-\frac{\beta_iM_{Li}}{\rho_i}[\sin(\beta_il_i)\cosh(\beta_il_i)-\cos(\beta_il_i)\sinh(\beta_il_i)]\\&-\frac{\beta_i^3J_{Li}}{\rho_i}[\sin(\beta_il_i)\cosh(\beta_il_i)+\cos(\beta_il_i)\sinh(\beta_il_i)]+\frac{\beta_i^4M_{Li}J_{Li}}{\rho_i^2}[1-\cos(\beta_il_i)\cosh(\beta_il_i)]\\&-\frac{(MD)_i^2\beta_i^4}{\rho_i^2}[1-\cos(\beta_il_i)\cosh(\beta_il_i)]-\frac{2(MD)_i\beta_i^2}{\rho_i}\sin(\beta_il_i)\sinh(\beta_il_i)\}\end{aligned} \tag{14}$$

$$\begin{aligned}\Delta_2=(EI)_i\beta_i\{&\cos(\beta_il_i)\sinh(\beta_il_i)-\sin(\beta_il_i)\cosh(\beta_il_i)-2\frac{M_{Li}\beta_i}{\rho_i}\sin(\beta_il_i)\sinh(\beta_il_i)-2\frac{J_{Li}\beta_i^3}{\rho_i}\cos(\beta_il_i)\cosh(\beta_il_i)\\&-\frac{M_{Li}J_{Li}\beta_i^4}{\rho_i}[\cos(\beta_il_i)\sinh(\beta_il_i)-\sin(\beta_il_i)\cosh(\beta_il_i)]-\frac{2(MD)_i\beta_i^2}{\rho_i}[\cos(\beta_il_i)\sinh(\beta_il_i)+\sin(\beta_il_i)\cosh(\beta_il_i)]\\&-\frac{(MD)_i^2\beta_i^4}{\rho_i^2}[\sin(\beta_il_i)\cosh(\beta_il_i)-\cos(\beta_il_i)\sinh(\beta_il_i)]\}\end{aligned} \tag{15}$$

It can be observed that (13) is a general form of the frequency equations derived for spring-hinged articulated rotor blades equation in [6] and the clamped-mass solution developed in [7].

The orthogonality conditions for two-link robot with elastic rotational restraints are given by [5]

$$\int_0^{l_i} \phi_{ij}(x_i)\rho_i\phi_{ik}(x_i)dx_i + \phi_{ij}(x_i)M_{Li}\phi_{ik}(x_i)\Big|_{x_i=l_i} + \frac{d\phi_{ij}(x_i)}{dx_i} J_{Li} \frac{d\phi_{ik}(x_i)}{dx_i}\Big|_{x_i=l_i} + (MD)_i \frac{d\left[\phi_{ij}(x_i)\phi_{ik}(x_i)\right]}{dx_i}\Big|_{x_i=l_i} = \begin{cases} 0 & j \neq k \\ P_i & j = k \end{cases} \quad (16)$$

And applying the boundary conditions

$$\int_0^{l_i} \frac{d^2\phi_{ij}(x_i)}{dx_i^2}(EI)_i \frac{d^2\phi_{ik}(x_i)}{dx_i^2}dx_i + \frac{d\phi_{ij}(x_i)}{dx_i}\sigma_{oti}\frac{d\phi_{ik}(x_i)}{dx_i}\Big|_{x_i=0} = \begin{cases} 0 & j \neq k \\ P_i\omega_{ij}^2 & j = k \end{cases} \quad (17)$$

The total kinetic energy of the two-link flexible robot with elastic rotational constraint is given by [8]

$$T = \frac{1}{2}\sum_{i=1}^{2}\rho_i\dot{P}_i^T\dot{P}_i dx + \frac{1}{2}\sum_{i=1}^{2}J_{hi}\,\dot{\alpha}_{i0}^T\dot{\alpha}_{io} + \frac{1}{2}m_{h2}\dot{P}_1^T\dot{P}_1\Big|_{x_1=l_1} + \frac{1}{2}m_p\dot{P}_2^T\dot{P}_2\Big|_{x_2=l_2} + \frac{1}{2}J_p\dot{\alpha}_p^T = \frac{1}{2}\dot{q}^T M\dot{q} \quad (18)$$

where M is the inertia matrix of the two-link flexible manipulator.

The potential energy of the two-link flexible manipulator with elastic rotational restraints is expressed as follows [9]:

$$V = \frac{1}{2}\sum_{i=1}^{2}\sum_{j=1}^{2}\sum_{k=1}^{2}\left\{\int_0^{l_i}\frac{\partial^2\phi_{ij(x_i)}}{\partial x_i^2}(EI)_i\frac{\partial^2\phi_{ik}}{\partial x_i^2}dx_i + \frac{\partial\phi_{ij(x_i)}}{\partial x_i}\sigma_{0ti}\frac{\partial\phi_{ik(x_i)}}{\partial x_i}\Big|_{x_i=l_i}\right\}\delta_{ij}\delta_{ik} \quad (19)$$

The closed-form is obtained through Lagrange-Euler equations expressed as

$$\frac{d}{dt}\frac{\partial L}{\partial\dot{q}_i} - \frac{\partial L}{\partial q_i} = f_i \quad (20)$$

where

$L = T - V$

$q = (\theta_1, \theta_2, \delta_{11}, \delta_{12}, \delta_{21}, \delta_{22})$

f_i is the vector of generalized forces.

The closed form dynamic equation can be written in a compact form as [4]

$$M(q)q + Dq + \ddot{K}\dot{q} = Qu \quad (21)$$

where

K is the stiffness matrix derived using (17) and (19)

u is the joint torque vector.

$D_{ij} = 0.1\sqrt{K_{ij}}$

$Q = [I_{n\times n}O_{n\times(N-n)}]^T$

$N = n + \sum_i m_i$

4. Simulation results

The dynamic model developed in the previous section is used to simulate the vibrational behaviour of a two-link flexible robot with the physical parameters given in Table 1. To assess the impact of the rotational stiffness coefficient of the actuator gearhead-link connections on the vibrational behaviour of the tip of the two-link system, dynamic simulations are conducted for various stiffness coefficients. The same stiffness coefficient is adopted for both joints. The natural frequencies obtained from the frequency equation (13) are summarized in Table 2. The clamped solution is obtained when $\sigma_{ot} \longrightarrow \infty$.

Table 1. Two- link flexible robot physical parameters.

Symbol	Parameter	Value	Unit
d	Specific weight	2666	kg/ m^3
m_1	Link 1 mass	0.165	kg
m_2	Link 2 mass	0.161	kg
m_{h2}	Hub 2 mass	0.347	kg
m_p	Payload mass	0.113	kg
l_1	Link 1 length	0.589	m
l_2	Link 2 length	0.575	m
$\boldsymbol{b = b_1 = b_2}$	Link thickness	0.035	m
$h_t = h_{t1} = h_{t2}$	Link height	0.003	m
$\boldsymbol{E}$	Modulus of elasticity	69	GPa
J_{01}	Link 1 moment of inertia	0.0191	kgm^2
J_{02}	Link 2 moment of inertia	0.0177	kgm^2
J_{h1}	Hub 1 moment of inertia	0.0001486	kgm^2
J_{h2}	Hub 2 moment of inertia	0.00041	kgm^2
$(EI) = (EI)_1 = (EI)_2$	Flexural rigidity	5.434	Nm^2
$P_1 = m_1$	Normalizing scale factor for link 1	0.165	kg
$P_2 = m_2$	Normalizing scale factor for link 2	0.161	kg

Table 2. Links 1 and 2 natural frequencies for various stiffness coefficients.

	Link 1		Link 2	
σ_{ot} [Nm/rad]	f_{11} [Hz]	f_{12} [Hz]	f_{21} [Hz]	f_{22} [Hz]
150	0.9303	6.0177	3.3229	31.5773
300	0.9612	6.1706	3.4742	32.8893
3000	0.9910	6.3466	3.6320	34.4734
∞	0.9963	6.3712	3.6471	34.7430

Different rotational stiffness coefficients are used to study the mode shapes of a two link flexible system. The results are shown in Figures 3 through 6.

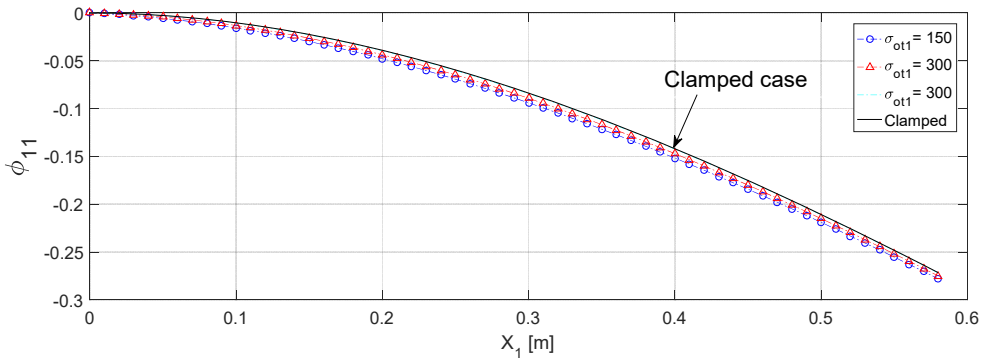

Fig. 3. Mode shapes Φ_{11} for various stiffnesses

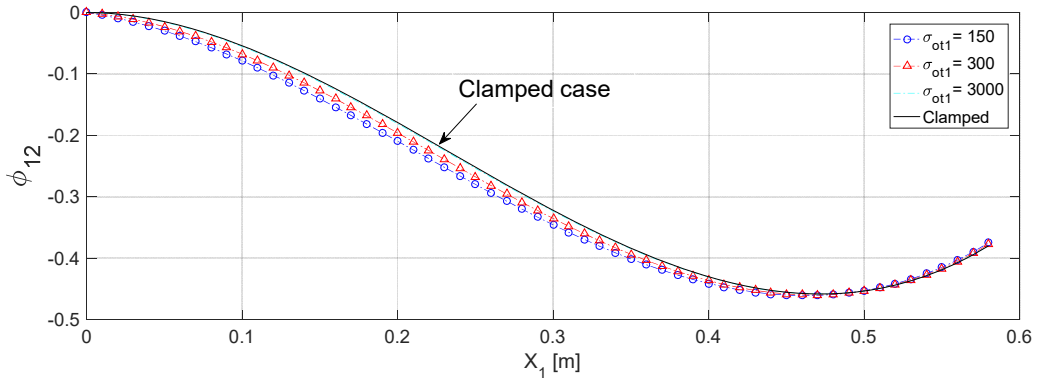

Fig. 4. Mode shape Φ_{12} for various stiffnesses

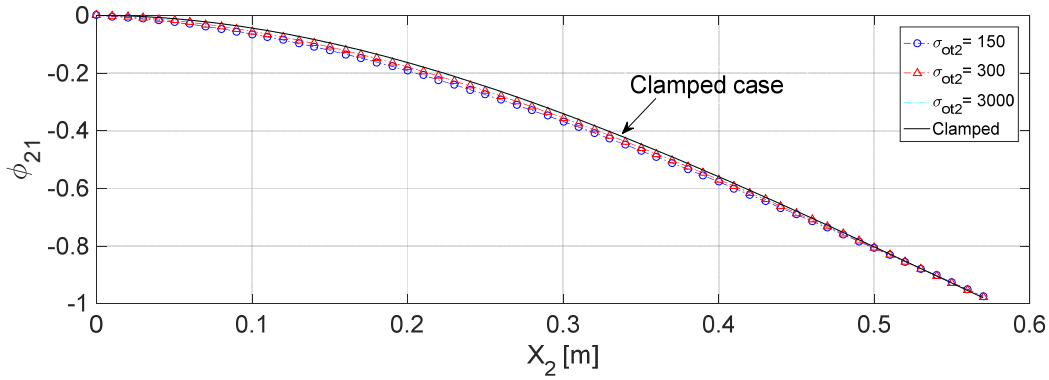

Fig. 5. Mode shapes Φ_{21} for various stiffnesses

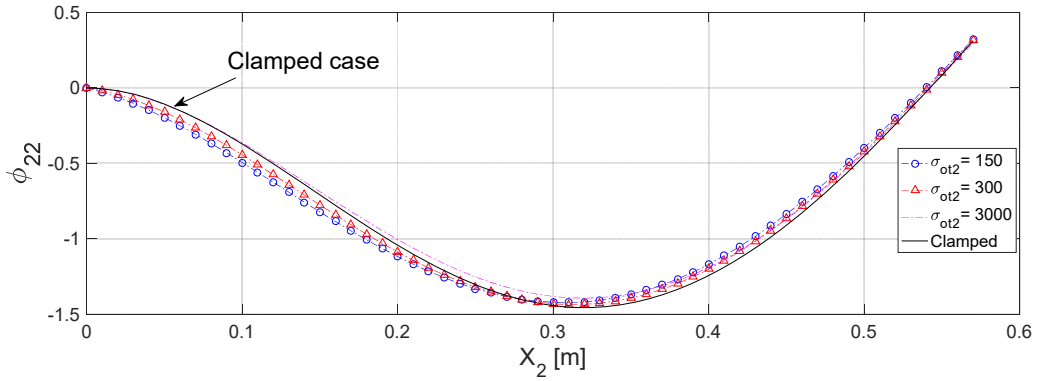

Fig. 6. Mode shape Φ_{22} for various stiffnesses

It can be noticed from Fig. 3 through 6 that a change in the rotational stiffness coefficients significantly affects the mode shapes of the system. It is noticeable that as the rotational stiffness coefficient increases, the mode shapes move toward the clamped end solution as the slope at the base of the link approaches zero.

To investigate the tip deflections, the arm is fully stretched and an initial 0.01 m deflection is given to the distal end of link 1 while maintaining the relative rotation angle between link 1 and link 2 zero. Fig. 7 shows the evolution of

relative rotation between link 1 and link 2 for various rotational stiffness coefficients. It can be noticed that initially, the static solutions coincide with the dynamic solutions.

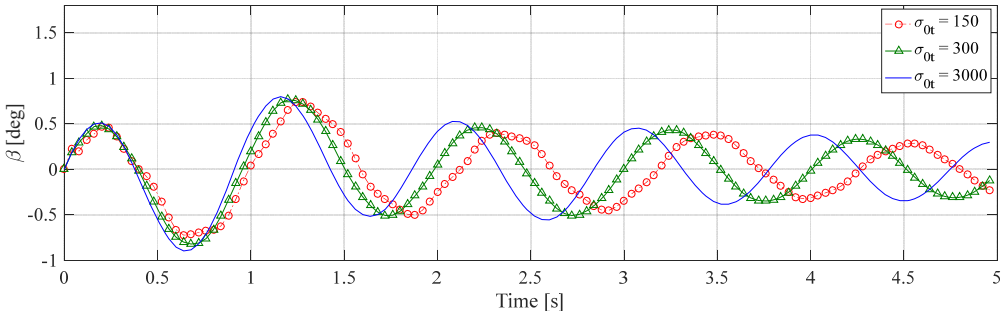

Fig. 7. Evolution of relative angle between link 1 and link 2.

The tip displacement is shown in Fig. 8. It can be observed that the higher the rotational stiffness coefficient, the higher the tip vibrational frequency. The highest frequency corresponding to the clamped mode solution is attained when the rotational stiffness coefficient approaches infinite. Therefore, in those situations where a joint with flexible constraint is modelled like one with a clamped end, the natural frequencies will be overestimated.

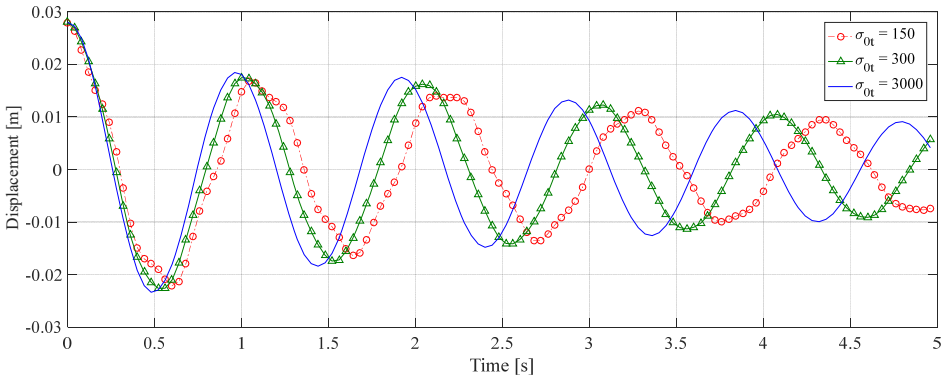

Fig. 8: Link 2 tip displacement

5. Conclusion

A dynamic modelling of planar flexible link robot with elastic restraint was presented. The assumed mode in conjunction with Lagrange formulation were used to derive the closed form dynamic equation of motion. Comparisons were conducted to assess the effect of hinge torsional stiffness coefficients on the tip vibrational behaviour through simulations. It was established that in those situations where there is a relative motion at the gearhead-shaft connection and the traditional clamped– mass solution might lead to overestimated system natural frequencies. The dynamic model proposed in this study covers all the ranges of flexibility from hinged-mass to clamped mass solution. The future work will involve the dimensionless analysis of the natural frequencies and mode shapes of planar flexible link with elastic rotational restraints at the actuator shaft gearhead-link connections.

References

1. McGuire, J. (1995) Notes on Semi- Rigid Connection. NASA Goddard Space Flight Center.
2. Oh, C. (1990) Modeling and control of a two- arm elastic robot in gravity. A doctoral thesis. Iowa State University, USA.
3. Belleza, F., Lanari, L. & Ulivi, G. (1990) Exact modelling of the flexible slewing link. *Proceedings of the IEEE international conference on Robotics and Automation*, 734- 739.

4. De Luca, A. & Siciliano, B. (1991) Closed form dynamic model of planar multilink lightweight robots. IEEE Transactions on Systems, Man and Cybernetics SMC- 21, 826- 839.
5. Tekweme, F.K. (2018) Parametric Study of Natural Frequencies and Mode Shapes of Planar Flexible-link Robots with Elastic Rotational Restraints at the Joint-Link Couplings. Unpublished paper.
6. Goulos, I., Pachidis, V. & Pilidis, P. (2014) Lagrangian formulation for the rapid estimation of helicopter rotor blade vibration characteristics. The Aeronautical Journal. 118 (1206), pp. 861- 901.
7 Tekweme, F.K & Nel, A. (2016) Parametric study of suitable orthogonality conditions for planar multilink flexible robots. *Proceedings of 10th South African Conference on Computational and Applied mathematics.* (2016), pp. 503- 512.
8 Tekweme, F. K. (2017) Dynamic modelling, Simulation and Input- Shaped Control of Planar Two-link Flexible Manipulators. Doctoral thesis. University of Johannesburg, RSA.
9 Grossi, R. O. & Albarracín, C. (2003) Eigenfrequencies of generally restrained beams, *Journal of Applied Mathematics*, 10:503-516, 2003.